Academic Journal of Science and Technology
ISSN: 2771-3032 | Vol. 20, No. 3, 2026

Preparation and Performance Study of Ultra-lightweight In-situ Self-foaming Composite Insulation Cores

Linyao Wu[1, *], Yunpeng Liu[1] and Le Li[1]

[1]Department of Electrical Engineering, North China Electric Power University, Baoding, China

***Corresponding author**: wulinyao2001@163.com

Abstract: To achieve the lightweighting of pillar composite insulators, this study employs an in-situ self-foaming molding process to prepare expandable microsphere/epoxy composite insulation core materials. Using DU658 expandable microspheres as fillers and E-51 epoxy resin as the matrix, the core density was controlled at 0.35 g/cm^3. Four types of specimens with resin mass fractions of 55%, 60%, 65%, and 70% were prepared. The effects of resin content on microscopic morphology (SEM), chemical structure (FT-IR), interfacial properties (dye penetration), thermal properties (DSC, TG, DMA), and power frequency breakdown strength were systematically investigated. Results indicate that resin content influences cell size and distribution by regulating the expansion space of microspheres and the matrix constraint. The 55% resin group exhibited the smallest cells with a concentrated distribution; the 65% group had the largest cell size and highest dispersion; the 70% group's cell distribution tended toward concentration again due to enhanced matrix encapsulation. FTIR testing confirmed that only physical bonding exists between the microspheres and the resin, with no chemical reaction. All specimens passed the dye penetration test, showing tight interfacial bonding. Regarding thermal properties, DSC results showed that the glass transition temperature increased from 85 ℃ to 109 ℃ with increasing resin content. TG analysis indicated that the initial decomposition temperature (T5%) of all specimens was above 192 ℃, making them suitable for long-term service below 200 ℃. DMA results showed the 60% resin group had the highest initial storage modulus (1250 MPa), satisfying rigidity requirements. Breakdown performance tests revealed a downward trend in power frequency breakdown strength as resin content increased; however, the breakdown strength of all specimens exceeded 30 kV/cm, meeting electrical standards, with the 55% resin group performing best. This study provides an experimental basis for the formulation and process optimization of lightweight insulation cores for UHV/EHV insulators.

Keywords: Pillar insulation core; expandable microspheres; composite foam; microscopic morphology; thermal properties; breakdown strength; in-situ self-foaming.

1. Introduction

With the rapid development of ultra-high voltage power transmission technology in China, the demand for lightweight and highly reliable power transmission and transformation equipment has become increasingly urgent[1-5]. As a core supporting component of electrical equipment[6,7], the performance of the internal insulating core of the composite post insulator directly determines the operational stability of the equipment[8]. Conventional insulating core materials are characterized by high density and complex processing, making it difficult to simultaneously achieve lightweight design and excellent electrical performance[9-13]. Driven by the demand for lightweight power transmission and transformation equipment, the development of ultra-lightweight composite core materials with high insulation performance has become a research hotspot[14-16]. Expandable microspheres are ideal fillers for ultra-lightweight insulation cores due to their foaming mechanism, which allows for the formation of uniform closed-cell structures within polymer matrices[17-21]. However, existing expandable microsphere-based insulation materials often utilize the traditional process of "foaming first, then infusion," which involves complex preparation procedures[22-24], low production efficiency[25-27], and issues such as poor interfacial bonding and stress concentration[28], making integrated core molding difficult. To address this, this study innovatively proposes an in-situ self-foaming molding process. Using DU658 expandable microspheres as fillers and E-51 epoxy resin as the matrix, ultra-lightweight composite foam cores with different resin mass fractions (55%–70%) were prepared through vacuum stirring, pre-curing, and stepped curing processes while maintaining a controlled density of 0.35 g/cm^3.

In this system, resin content is a key formulation parameter determining the ratio of the two phases and has a critical impact on cell morphology, interfacial bonding, and material properties. This paper focuses on the effects of resin mass fraction on the microscopic morphology (SEM) and cell size distribution, chemical structural characteristics (FT-IR), interfacial properties, thermal properties (DSC, TG, DMA), and power frequency breakdown strength of the composite foam cores. The goal is to analyze the influence of resin content on the microstructure and key properties, providing an experimental basis for the formulation optimization and process design of lightweight insulation cores for UHV/EHV insulators.

2. Specimen Preparation and Testing Methods

2.1. Raw Materials

E-51 epoxy resin (diglycidyl ether of bisphenol A, DGEBA) produced by Nantong Phoenix Petrochemical was used; its molecular structure and 3D model are shown in Figure 1a, with an epoxy value of 0.51 mol/100 g. Methylhexahydrophthalic anhydride (MeHHPA) with a

purity of 95% was selected as the curing agent. Tris(dimethylaminomethyl)phenol (DMP-30) with a purity of 95% was used as the accelerator. EXPANCEL® DU658 polymer microspheres were selected as the lightweight filler. These expandable microspheres feature a thermoplastic shell-core structure with an unexpanded average particle size of 22-32 μm, primarily composed of methyl methacrylate/acrylonitrile copolymer (MMA/AN copolymer), isopentane, and isooctane. The molecular structure and 3D model of the MMA/AN copolymer are shown in Figure 1b.

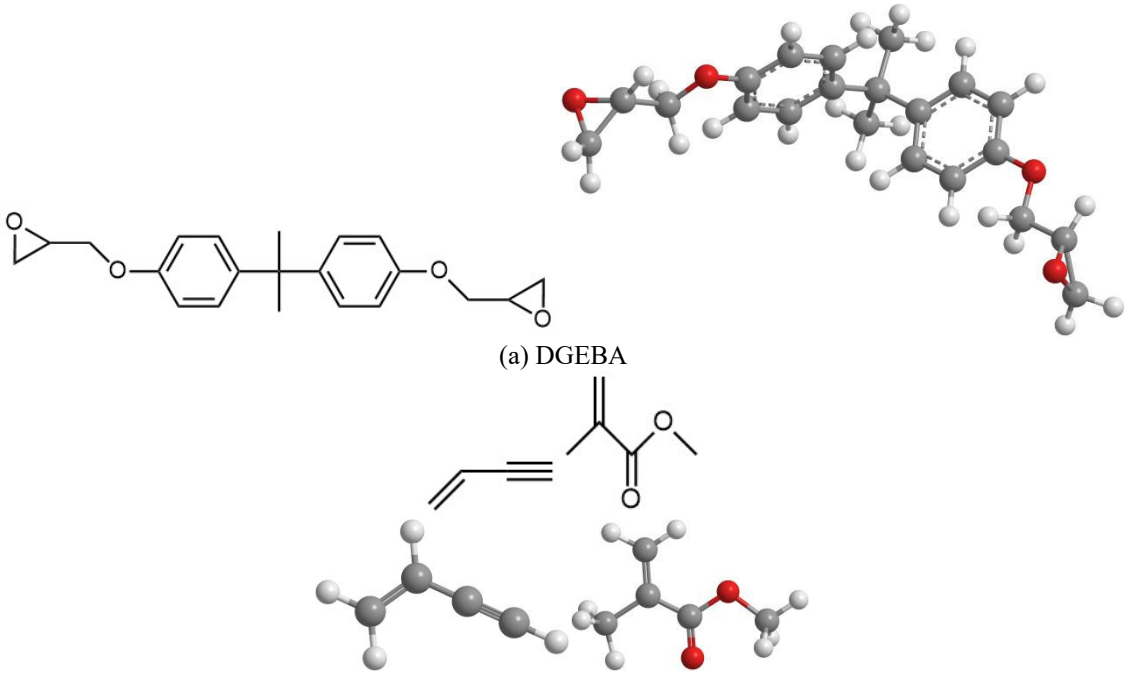

(a) DGEBA

(b) MMA/AN copolymer

Figure 1. Molecular structures and 3D models of key materials

2.2. Specimen Preparation

Utilizing the in-situ self-foaming molding process, DGEBA, MeHHPA, DMP-30, and unexpanded DU658 microspheres were mixed according to the design proportions, with resin mass fractions set at 55%, 60%, 65%, and 70%. The mixture was placed in a planetary mixer (Maolixi, MT-300) and stirred at 600 r/min for 20 min under vacuum to ensure uniform dispersion of all components. This was followed by vacuum pre-curing at 70 ℃ for 1 h to moderately increase the viscosity of the epoxy system, effectively preventing microsphere agglomeration or precipitation before subsequent foaming while further removing residual gases to obtain a uniformly mixed liquid composite foam. Finally, the liquid composite foam was poured into a cylindrical stainless steel mold that had been coated with a release agent and preheated to 80 ℃ for foaming and curing.

The foaming mechanism of expandable microspheres is as follows: upon heating, the thermoplastic resin (MMA/AN copolymer) forming the microsphere shell softens, while the encapsulated liquid hydrocarbon blowing agents (isopentane, isooctane) vaporize, leading to a sharp increase in internal pressure. When the internal gas pressure reaches a dynamic equilibrium with the tension of the softened shell and the external environmental pressure, the microspheres maintain an expanded equilibrium state, forming a balloon-like closed-cell structure. Overheating may cause gas to escape through the thinned shell, leading to microsphere shrinkage. Therefore, the temperature and time for foaming and curing must be precisely controlled.

This study controlled the final density of the core material at 0.35 g/cm³ by using stainless steel molds of fixed volume and maintaining a fixed total mass of the fillers. The specific foaming and curing process was: foaming at 180 ℃ for 1 h to allow the microspheres to expand fully and fill the mold; followed by stepped cooling curing, first at 120 ℃ for 2 h, then at 100 ℃ for 1 h. Finally, the samples were naturally cooled to room temperature before demolding. The specific preparation process is shown in Figure 2. The retrieved specimens were cut into sizes of 30 mm, 10 mm, 2 mm, etc., for subsequent performance testing.

2.3. Characterization and Testing Methods

2.3.1. Microstructural Analysis

A FEI Nova Nano-450 Scanning Electron Microscope (SEM) was used to observe the microscopic structural state of the composite foam insulation core and its interface. During sample preparation, the specimens were cryogenically fractured under liquid nitrogen, and the cross-sections were sputter-coated with gold twice (3 mA, 1 min) to eliminate charging effects. Observations were conducted in secondary electron mode (SE mode) under high vacuum conditions, with an activation voltage of 10 kV and a working distance of 10 mm. Fourier Transform Infrared Spectroscopy (FTIR) analysis was performed on the composite foam insulation material specimens using a Thermo Nicolet NEXUS 870 (6 700) spectrometer to characterize the chemical structure of the core material. The scanning range was 4,000 to 400 cm^{-1}, observing the characteristic absorption peaks of the corresponding functional groups.

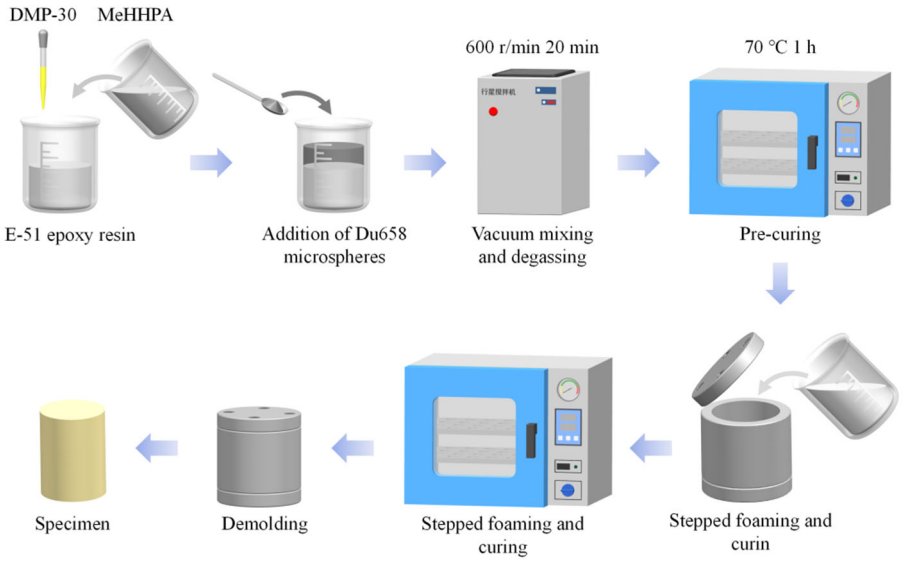

Figure 2. Preparation flow chart of self-foaming epoxy-based composite foam insulation core

2.3.2. Interfacial Performance Characterization

A glass container was filled with steel balls 2 mm in diameter, and an ethanol solution containing 1% magenta dye was poured into the container until the liquid level was 2 mm to 3 mm above the top of the balls. Core samples with a height of 10 mm were then placed on the steel balls for dye penetration testing.

2.3.3. Electrical Performance Testing

AC breakdown strength is a key indicator for evaluating the insulation performance of composite foam cores, reflecting the material's ability to resist breakdown under strong electric fields. The test was conducted in transformer oil. Specimens with a thickness of (2 ± 0.1) mm were used. Sphere electrodes were placed at the center of the composite foam material, and the voltage was gradually increased at a rate of 1 kV/s until breakdown occurred. The breakdown voltage of the core material was recorded. Ten tests were performed for each group of samples, and the breakdown strength was analyzed using the Weibull distribution.

2.3.4. Thermal Performance Testing

Differential Scanning Calorimetry (DSC) was used to study the curing behavior and glass transition temperature (T_g) of the composite foam cores to evaluate the effect of resin content on the thermal transition characteristics of the material. Testing was performed using a Netzsch DSC 3500 Sirius calorimeter under a nitrogen protective atmosphere with a flow rate of 20 mL/min. The testing temperature range was -20 °C to 220 °C, with a heating rate of 10 K/min.

Thermal stability is an important factor determining the application of epoxy resin. Thermogravimetric Analysis (TGA) is a convenient and common method for characterizing the thermal stability and components of polymer materials. Thermal weight loss was tested using a Mettler-Toledo TGA/DSC 3 thermogravimetric analyzer. Test conditions: the specimen was placed in an Al_2O_3 crucible and tested in a nitrogen atmosphere at a heating rate of 10 °C/min, with a temperature range from 30 °C to 800 °C.

Dynamic Mechanical Analysis (DMA) was used to study the dynamic mechanical properties of the composite foam cores at different temperatures, including storage modulus (E'), loss modulus (E''), and loss factor (tanδ), to evaluate the impact of resin content on the rigidity and glass transition behavior of the material. Testing was conducted using a TA-DMA 850 analyzer in single cantilever beam mode, with a test frequency of 2 Hz, a heating rate of 5 °C/min, and a temperature range from 30 °C to 200 °C.

3. Results and Discussion

3.1. Microscopic Morphology (SEM) Analysis

The SEM morphology and particle size distribution of the cross-sections for specimens with different resin contents are shown in Figure 3. Image-J image analysis software was used to manually label and automatically measure no fewer than 100 cells in each SEM image. The average particle size and standard deviation were statistically calculated, and the ratio of the standard deviation to the average particle size was used as the coefficient of variation (*CV*) to evaluate the uniformity of the cell size distribution in core specimens with different resin contents. The *CV* is used to quantitatively evaluate the uniformity of the cell size distribution; a smaller *CV* indicates a more concentrated distribution. As the resin content increased from 55% to 65%, the average cell size gradually increased, and the *CV* rose from 0.197 to 0.209, showing a more dispersed distribution. The 55% group had a *CV* of 0.197, with the smallest and most concentrated cells and no damage, which is attributed to the high proportion of microspheres, small spacing, and strong mutual constraint. The 65% group had the largest average particle size (56.70 μm) and the highest *CV* (0.209), with some damaged cells because the increased resin continuous phase provided more expansion space and weakened constraints for the microspheres. In the 70% group, the average particle size slightly decreased to 56.05 μm, and the *CV* dropped to 0.168 (the lowest of the four groups), with regular cell morphology, indicating that excessively high resin content enhances matrix encapsulation, inhibits over-expansion, and causes the distribution to concentrate again. SEM results demonstrate that resin mass fraction governs the evolution of the cell structure by affecting microsphere constraint and expansion space.

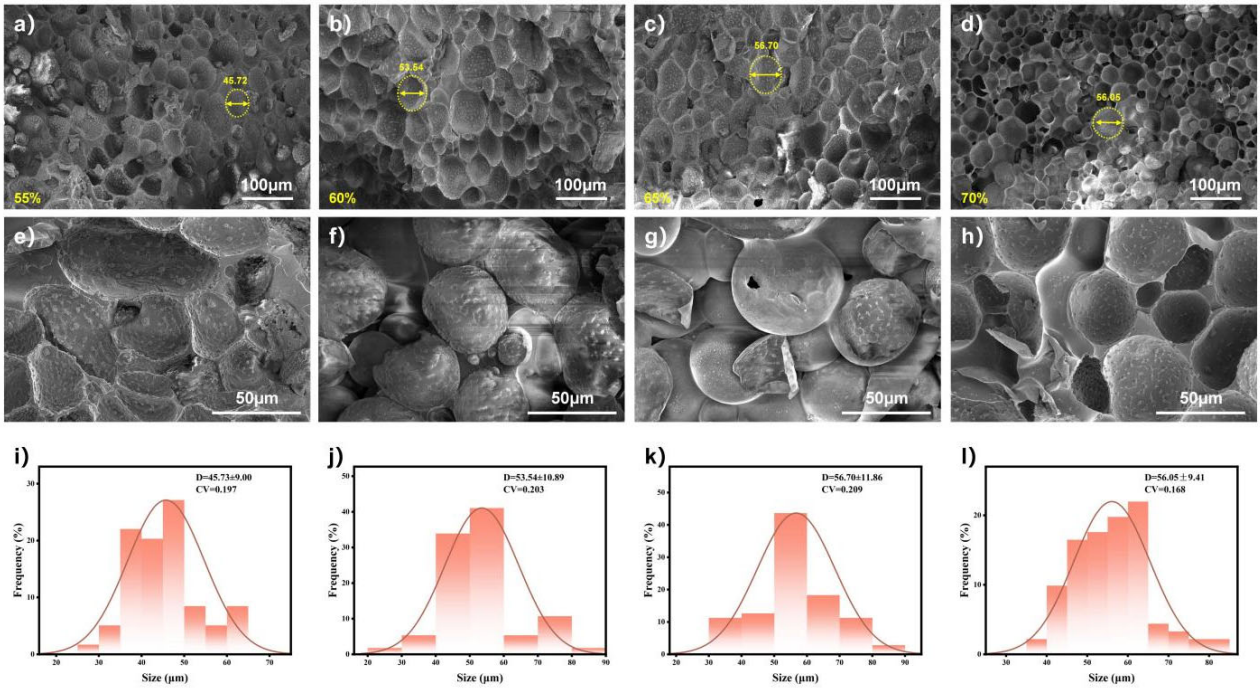

Figure 3. Interfacial microscopic morphology and particle size distribution of core specimens (a-d, e-h: interfacial microscopic morphology for 55-70% resin content; i-l: particle size distribution for 55-70% resin content)

3.2. Chemical Structure Analysis

The FT-IR spectra of core specimens with different resin contents are shown in Figure 4. The characteristic absorption peak positions were consistent for all specimens: the region around 3450–3463 cm^{-1} corresponds to hydroxyl (-OH) stretching vibration (from epoxy curing and adsorbed water); 2956 cm^{-1} and 2870 cm^{-1} are C-H stretching vibrations; 1731 cm^{-1} is the ester group C=O stretching vibration, originating from the anhydride-cured epoxy and the MMA/AN copolymer of the microsphere shell; 1609 cm^{-1} and 1510 cm^{-1} are benzene ring skeleton vibrations; and 1043 cm^{-1} is the aromatic ether C-O-C stretching vibration. As resin content increased, the intensity of the hydroxyl and ester peaks slightly strengthened, but no new characteristic peaks appeared, indicating that only physical bonding occurs between the expandable microspheres and the epoxy resin, with no chemical reaction.

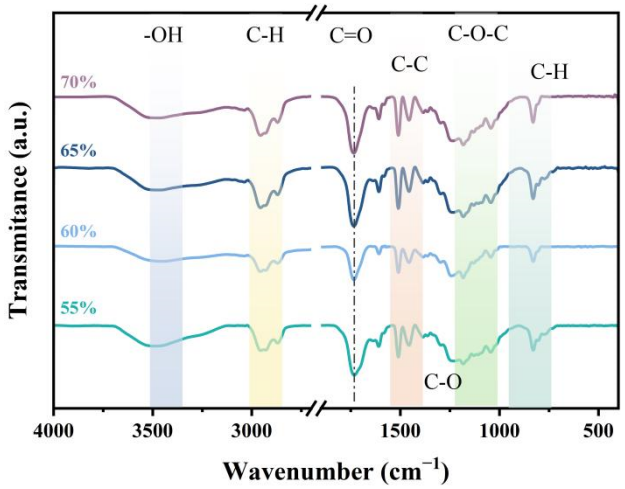

Figure 4. Fourier Transform Infrared spectra of core specimens with different resin contents

3.3. Interfacial Performance Analysis

The dye penetration test is an intuitive method for evaluating the interfacial integrity of composite materials. Figure 5 shows the images of the top end-face status of each core specimen after 15 min of dye penetration. No dye penetration paths were found inside any of the specimens, indicating that the cell structures are intact and the interface between the microspheres and resin is tightly bonded. This effectively blocked the capillary penetration of the dye, meeting the anti-penetration requirements for insulation cores and demonstrating good overall interfacial performance. From the perspective of the preparation process, the in-situ self-foaming process played a key role in interfacial optimization: vacuum high-speed stirring ensured uniform dispersion of the microspheres; pre-curing at 70 ℃ moderately increased resin viscosity to prevent layering and formed elastic constraints during the foaming stage, allowing

the matrix to deform synchronously with the microsphere expansion to achieve a tight fit; and stepped curing effectively eliminated internal stress and reduced interfacial micro-cracks. The combined effect of these processes ensured that even though individual cell damage existed in the 65% and 70% groups, the overall interfacial integrity remained good. The excellent interfacial performance provides an important guarantee for the reliable bonding of the core to the silicone rubber sheds/sheaths.

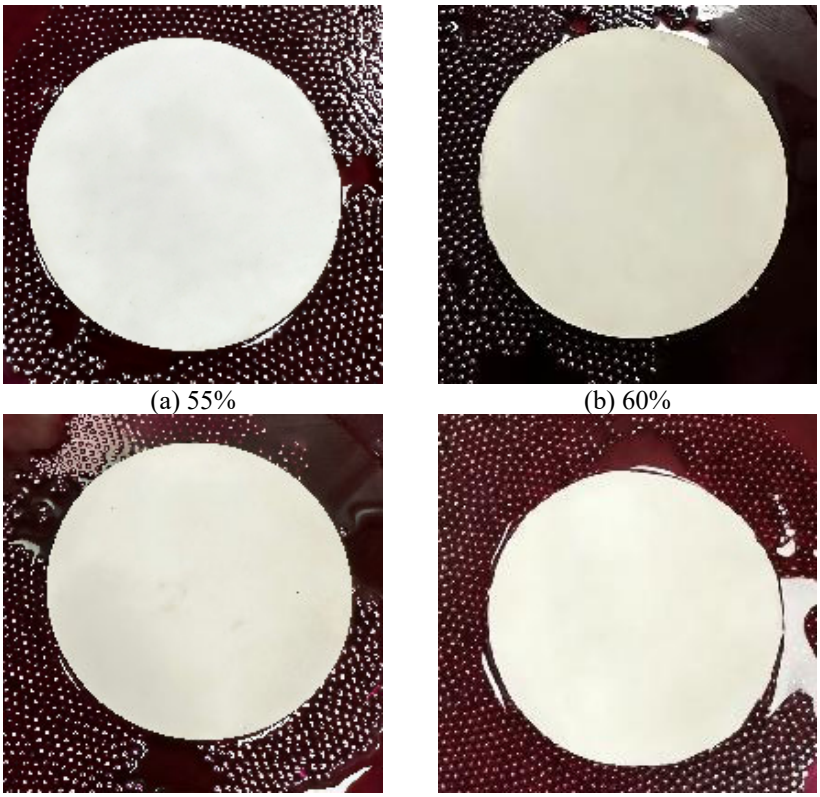

(a) 55% (b) 60%

(c) 65% (d) 70%

Figure 5. Condition of core specimens with different resin contents after the dye penetration test

3.4. Thermal Performance Analysis

3.4.1. DSC Analysis

The DSC curves of core specimens with different resin contents are shown in Figure 6. The glass transition temperature (T_g) corresponds to the transition of the cured epoxy from a glassy state to a high-elastic state. As resin content increased, the T_g gradually rose from 85 ℃ for the 55% group to 109 ℃ for the 70% group, indicating an increase in cross-linking density and restricted molecular chain movement. All samples exhibited an endothermic peak at 390-400 ℃, corresponding to the thermal decomposition of the epoxy resin matrix. The enthalpy values showed a trend of increasing first and then decreasing: 298.2 J/g for the 55% group, 388.1 J/g for the 60% group, reaching a peak of 830.3 J/g for the 65% group, and dropping to 545.9 J/g for the 70% group. The 65% group had the highest enthalpy value, attributed to moderate resin content, cell dispersion promoting heat conduction, and sufficient functional group reactions[29]; the 70% group showed a decrease in enthalpy due to restricted molecular chain movement and uneven reactions caused by excessively high cross-linking density.

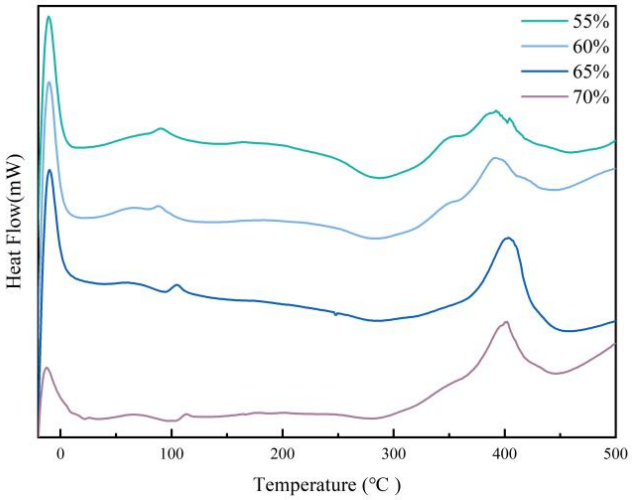

Figure 6. DSC curves of core specimens with different resin contents

3.4.2. TG Analysis

The thermogravimetric curves of core specimens with different resin contents are shown in Figure 7, with data summarized in Table 1. The thermal decomposition of all samples occurred in two stages: the first stage (200-300 ℃) had a weight loss rate of 16%-19%, corresponding to the rupture of the microsphere shells and the escape of blowing agents, which decreased from 19.0% to 16.0% as resin content increased; the second stage (300-500 ℃) had a weight loss rate of 66%-72%, corresponding to the cleavage of the epoxy resin main chain, with the 65% group showing the highest weight loss (72.3%), consistent with this group having the most complete curing (highest DSC enthalpy).

Regarding thermal stability, the initial decomposition temperature ($T_{5\%}$) ranged from 192-200 ℃, decreasing slightly as resin content increased; all specimens were above 190 ℃, allowing for long-term service below 200 ℃. The first DTG peak temperature (microsphere decomposition) dropped from 207 ℃ to 195 ℃ due to restricted microsphere expansion at high resin content; the second peak temperature (resin cleavage) rose from 380 ℃ to 391 ℃ (65% group), reflecting that increased cross-linking density inhibits main chain cleavage[30]. The residual mass at 600 ℃ was 10.8%-14.8%, with the 65% group being the lowest (10.8%), indicating the most thorough thermal decomposition.

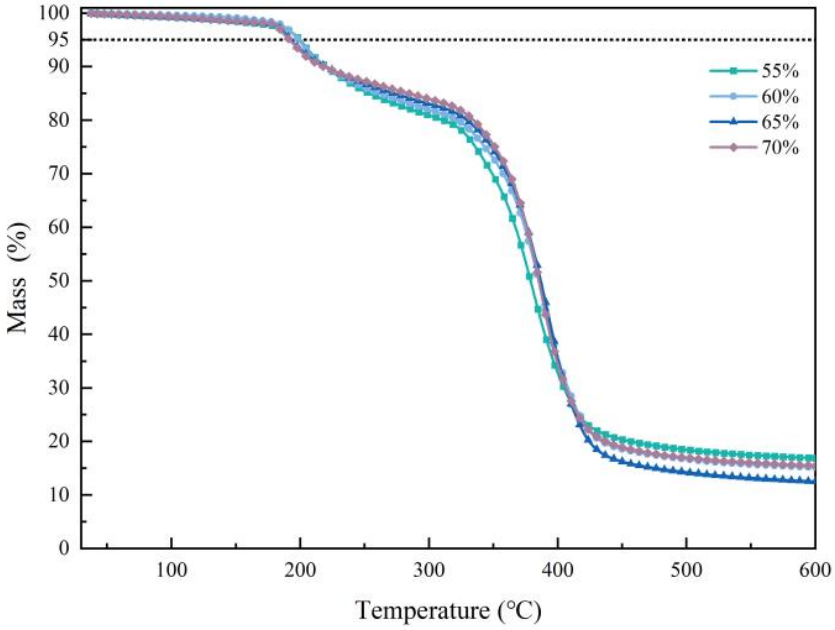

Figure 7. Thermogravimetric analysis curves of core specimens with different resin contents

Table 1. Thermogravimetric data of core specimens with different resin contents

Resin Mass Fraction	Initial Decomposition Temperature $T_{5\%}$ (℃)	First-stage Weight Loss Rate Δm_1 (%)	Second-stage Weight Loss Rate Δm_2 (%)	DTG Peak Temperature 1 T_{max1} (℃)	DTG Peak Temperature 2 T_{max2} (℃)	Residual Mass m_{res} (%)
55%	200	19.0	66.2	207	380	14.8
60%	199	18.1	68.3	203	387	13.6
65%	193	16.9	72.3	195	391	10.8
70%	192	16.0	70.1	195	386	13.9

3.4.3. DMA Analysis

Dynamic Mechanical Analysis (DMA) was used to characterize the viscoelastic behavior of the composite foam cores, obtaining the variation laws of storage modulus (E'), loss modulus (E''), and loss factor (tanδ) with temperature. Figure 8 shows the DMA curves for the four types of specimens. In the low-temperature region (20-80 ℃, in the glassy state), there were significant differences in storage modulus: the 55% group was the lowest (300-400 MPa) due to the high proportion of microspheres and less resin continuous phase; the 60% group was the highest (900-1300 MPa), attributed to the dense epoxy cross-linking network, uniform cells (CV=0.203), and good interfacial bonding; the 65% and 70% groups were 400–600 MPa and 400–800 MPa respectively, with the drop in modulus related to cell damage and increased brittleness from high cross-linking[31]. After entering the glass transition region, E' decreased significantly, and tanδ reached its peak. The tanδ peak temperature (T_g, DMA) rose monotonically with increasing resin content: approximately 100 ℃ for the 55% group, 102 ℃ for the 60% group, 113 ℃ for the 65% group, and 120 ℃ for the 70% group, consistent with the DSC trend (though values were higher, following the time-temperature superposition principle). No multiple peaks were observed in the tanδ curves of any specimens, indicating no phase separation and tight interfacial bonding between the microspheres and the resin.

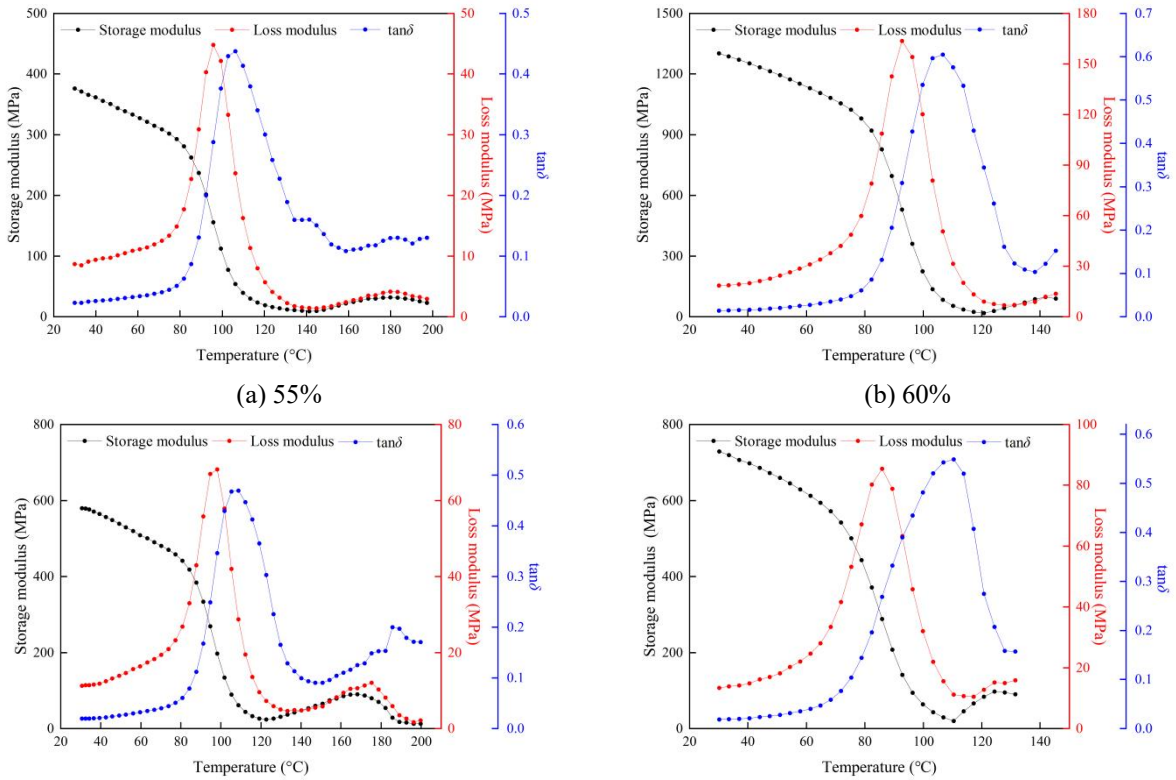

(a) 55% (b) 60%

(c) 65% (d) 70%

Figure 8. DMA curves of core specimens with different resin contents

3.5. Breakdown Strength Analysis

Breakdown strength reflects the composite foam core's ability to withstand electric fields. Figure 9 shows the Weibull distribution plots for the four groups, with analysis focused on the characteristic breakdown strength corresponding to a 63.2% breakdown probability. The characteristic breakdown strengths for the 55%, 60%, 65%, and 70% resin groups were 21.7, 19.3, 16.4, and 12.7 kV/mm, respectively, all significantly higher than the 3 kV/mm required by the DL/T 1580-2016 standard, indicating engineering application potential even at ultra-low density (0.35 g/cm^3).

A clear downward trend in breakdown strength was observed as resin content increased. Combined with SEM analysis, the 55% group had the smallest cells (45.73 μm) which were intact, allowing the cell interfaces to consume discharge energy and lengthen the breakdown path, resulting in the highest breakdown strength[32]. In the 60% group, cells enlarged (53.54 μm) and the resin layer narrowed, leading to a decrease in breakdown strength. The 65% group had the largest cells (56.70 μm) with partial damage and an uneven resin layer, causing the breakdown strength to drop further to 16.4 kV/mm. Although the 70% group had a concentrated cell size distribution (*CV*=0.168), the cells were large (56.05 μm) and exhibited damage, resulting in the lowest breakdown strength (12.7 kV/mm), a 41.5% decrease compared to the 55% group. In summary, the small size and integrity of the cells have a greater impact on breakdown strength than the resin content itself, making them key to enhancing electrical performance.

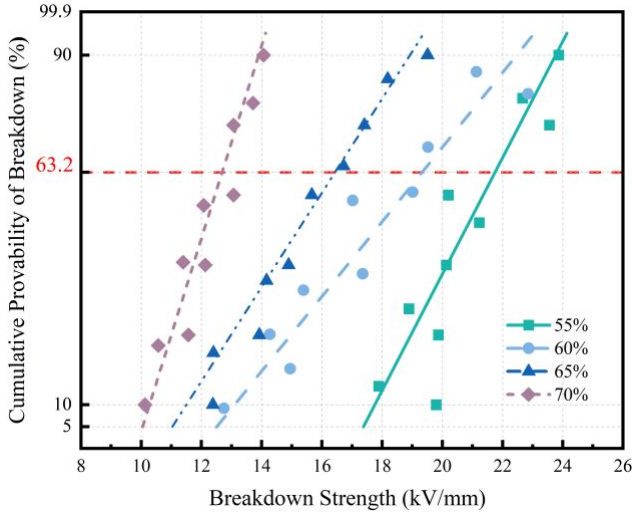

Figure 9. Weibull distribution of breakdown strength for core specimens with different resin contents

4. Conclusion

(1) Ultra-lightweight composite insulation cores with a density of 0.35 g/cm^3 were successfully prepared using the in-situ self-foaming molding process. Resin mass fraction influences cell structure evolution by regulating microsphere expansion space and matrix constraint: the 55% group had the smallest cells (45.73 μm) and the most concentrated distribution (CV=0.197); the 65% group had the largest cells (56.70 μm) and the highest dispersion (CV=0.209); and the 70% group showed a re-concentrated distribution (CV=0.168) due to strong matrix constraints. FTIR confirmed only physical bonding between microspheres and resin, with no chemical reaction.

(2) All specimens passed the dye penetration test, with no dye penetration paths inside the cores, indicating intact cell structures, tight bonding at the microsphere-resin interface, and excellent closed-cell performance. The synergistic effects of vacuum stirring, pre-curing, and stepped curing in the in-situ self-foaming process effectively eliminated internal stresses and reduced interfacial micro-cracks, providing an important guarantee for the reliable bonding between the core and the silicone rubber sheds.

(3) Regarding thermal properties, DSC showed the glass transition temperature increased from 85 ℃ to 109 ℃ with increasing resin content, with the 65% group having the highest enthalpy value (830.3 J/g). TG analysis indicated the initial decomposition temperature ($T_{5\%}$) for all specimens was above 192 ℃, allowing for long-term service below 200 ℃. DMA showed the 60% group had the highest initial storage modulus (1250 MPa), meeting rigidity requirements, and no phase separation was observed in any specimens.

(4) Breakdown strength showed a downward trend as resin content increased. The characteristic breakdown strengths for the 55%, 60%, 65%, and 70% resin groups were 21.7, 19.3, 16.4, and 12.7 kV/mm, respectively, all far exceeding the 3 kV/mm required by the DL/T 1580-2016 standard. The 55% group exhibited the best breakdown performance due to its fine and intact cells. Research indicates that cell size and integrity have a greater impact on electrical performance than the resin content itself, providing an experimental basis for formulation optimization of lightweight insulation cores for UHV/EHV insulators.

The in-situ self-foaming molding process innovatively proposed in this study, which involves direct mixing of unexpanded expandable microspheres with epoxy resin and other raw materials followed by vacuum stirring, pre-curing, and one-step foaming/curing, successfully solves the technical challenges of the traditional "foaming first, then infusion" process, such as complexity, poor interfacial bonding, and difficulty in integrated molding. The prepared epoxy composite foam core density can be controlled to 0.35 g/cm^3, achieving the core objective of ultra-lightweighting. Furthermore, the core possesses good electrical, thermal, and dynamic mechanical properties, providing an experimental basis for the formulation optimization and process design of high-performance lightweight insulation cores for UHV/EHV insulators, helping to drive the development of power transmission and transformation equipment toward lightweighting and high reliability.

Acknowledgements

The authors gratefully acknowledge the financial support from the Fundamental Research Funds for the Central Universities (2025MS107) and Hebei Provincial Higher Education Institutions Scientific Research Project (BJ2026255).

References

[1] Li Peng, Wang Rui, Ji Haoran, et al. Research and prospect of planning for low-carbon smart distribution network[J]. Automat ion of Electric Power Systems, 2021, 45(24): 10-21.(inChinese)

[2] Zhang Sheng. Prospects of China's Petroleum Refining and Petrochemical Industry under “Dual Carbon” Goals[J]. China Oil & Gas, 2022, 29(3): 41-46.

[3] Yun Baoji, Zhang Enshuo, Zhang Guo, et al. Optimal operation of anintegrated energy system consideringinte-grated demandresponse and a ‘dual Carbon’ mechanism[J]. Power System Protection and Control, 2022, 50(22): 11-19. (inChinese)

[4] SHANG Yong, WANG Zhe, YAN Huan, et al. Research exploration of Shanxi new type power system in the background of ‘dual Carbon’[J]. Power System and CleanEnergy, 2023, 39(12): 20-27. (inChinese)

[5] Zeng Peng, Wen Xiankui1, Tan Zhukui, et al. Analysis of the Evolution and Development of China’s Power System Under the Goal of Carbon Peaking and Carbon Neutrality Goals[J]. Construction Economy, 2023, 44(S02): 33-37.(inChinese)

[6] Liu Y P, Zhang M J, Liu H C, et al. The influences of silane coupling agents on the heat and moisture resistance of basalt fibre-reinforced composites[J]. High Voltage, 2022, 8(1): 38-47.

[7] Yin Chengfeng, Xiao Zhang, Guo Yujun, et al. Method for detecting the pollution degree of naturally contaminated insulator based on hyperspectral characteristics[J]. High Voltage, 2021, 6(6): 1031-1039.

[8] Afolabi Olusegun A., Kanny Krishnan, Mohan T. P. Processing of Hollow Glass Microspheres (HGM) filled Epoxy Syntactic Foam Composites with improved Structural Characteristics[J]. Science and Engineering of Composite Materials, 2021, 28(1): 116-127.

[9] Sheng Wang Qun, Li Gang, Li Yanzhe, et al. Comprehensive simulation of snow crystal deposition and electric field characteristics of composite sheath improved porcelain cantilever insulator in a wind and snow environment[J]. Journal of Measurement Science and Instrumentation, 2022, 13(4): 379-389.

[10] Yang Xi, Wang Qingyu, Wang Haoran, et al. Transient electric field computation for composite cross-arm in 750kV AC transmission line under lightning impulse voltage[J]. IEEE Transactions on Dielectrics and Electrical Insulation, 2016, 23(4): 1942-1950.

[11] Kopparthi N R, Schuster J, Shaik Y P. Fabrication and Characterization of Bamboo—Epoxy Reinforced Composite for Thermal Insulation[J]. Open Journal of Composite Materials, 2024, 14(1): 15-32.

[12] Dong Weiwei ,Qian Danbo ,Xi Ying, et al.Preparation and properties of waterborne polyurethane coatings containing polyurethane-coated hollow glass microspheres[J].Progress in Organic Coatings, 2025, 208109490-109490.

[13] Liu Yunpeng, Li Le, Liu Hechen, et al. Hollow polymeric microsphere-filled silicone-modified epoxy as an internally insulated material for composite cross-arm applications[J]. Composites Science and Technology, 2020, 200(4): 108418.

[14] Wang Pucheng, Yang Na, Liu Dong, et al. Coupling effects of gamma irradiation and absorbed moisture on silicone foam[J]. Materials & Design, 2020, 195(1): 108998.

[15] Martin-Gallego M, Lopez-Hernandez E, Pinto J, et al. Transport properties of one-step compression molded epoxy nanocomposite foams[J]. Polymers, 2019, 11(5): 756-756.

[16] Song W, Tagarielli V L, Lee K Y. Enhancing the fracture resistance and impact toughness of mechanically frothed epoxy foams with hollow elastomeric microspheres [J]. Macromolecular Materials and Engineering, 2018, 303(12): 1800363.

[17] Stefani P, Barchi A T, Sabugal J, et al. Characterization of epoxy foams[J]. Journal of Applied Polymer Science, 2003, 90(11): 2992-2996.

[18] Cheng Qiyun, Sun Caixin, Zhang Xiaoxing, et al. Short-Term load forecasting model and method for power system based on complementation of neural network and fuzzy logic. Transactions of China Electrotechnical Society, 2004, 19(10): 53-58.

[19] Roggendorf C, Schnettler A. Accelerated hydrothermal aging of epoxy resin based syntactic foams with Polymeric Microspheres. IEEE Transactions on Dielectrics and Electrical Insulation, 2012, 19(3): 973-980.

[20] Yu Wei, Qian Meng, Li Huijian. Elastic and plastic properties of epoxy resin syntactic foams filled with hollow glass microspheres and glass fibers[J]. Journal of Applied Polymer Science, 2016, 133(46): 44188.

[21] Kessler M, Schnettler A. Investigation of the DC breakdown mechanism in elastic syntactic foams[J]. IEEE Transactions on Dielectrics and Electrical Insulation, 2010, 17(3): 898-905.

[22] Li Xiudi, Zhu Ming, Tang Xuemei, et al. Influence of hollow carbon microspheres of micro and nano-scale on the physical and mechanical properties of epoxy syntactic foams[J]. Rsc Advances, 2015, 5(63): 50919-50928.

[23] Wu Xinfeng, Tang Bo, Yu Jinhong, et al. Preparation and investigation of epoxy syntactic foam (epoxy/graphite reinforced hollow epoxy macrosphere/hollow glass microsphere composite)[J]. Fibers and Polymers, 2018, 19: 170-187.

[24] Bharath K B, Doddamani M, Zeltmann S E, et al. Effect of particle surface treatment and blending method on flexural properties of injection-molded cenosphere/HDPE syntactic foams[J]. Journal of materials science, 2016, 51: 3793-3805.

[25] Rousseau C-E, Plume G, Goñi M, et al. Behavior of syntactic foam under plate impact[J]. Mechanics Research Communications, 2017, 83: 1-5.

[26] Kaur M, Jayakumari L S. Consequence of cenosphere loading on hygrothermal, thermal, and mechanical properties of epoxy syntactic foams[J]. Journal of Cellular Plastics. 2019, 55(3):297-318.

[27] Samsudin S S, Ariff Z M, Zakaria Z, et al. Development and characterization of epoxy syntactic foam filled with epoxy hollow spheres[J]. Express Polymer Letters. 2011, 5(7).

[28] Ozkutlu M, Dilek C, Bayram G J C S. Effects of hollow glass microsphere density and surface modification on the mechanical and thermal properties of poly (methyl methacrylate) syntactic foams[J]. Composite Structures, 2018, 202: 545-550.

[29] Zheng Luyu, Wu Mei, Sun Dayu, et al. Development of a flame-retardant epoxy resin with high glass transition temperature and transparency based on a diphenylphosphine oxide derivative[J]. Frontiers of Chemical Science and Engineering, 2025, 19(8): 33-44.

[30] Lakouraj M M, Rahpaima G, Zare N E. Effect of functionalized magnetite nanoparticles and diaminoxanthone on the curing, thermal degradation kinetic and corrosion property of diglycidyl ether of bisphenol a-based epoxy resin[J]. Chinese Journal of Polymer Science, 2014, 32(11): 1489-1499.

[31] Jiang Shuajun, Meng Weifeng, Wan Yongqing, et al. Pyrolysis Mechanism of a cyclotriphosphazene-based flame-retardant epoxy resin by reaxFF molecular dynamics[J]. China Petroleum Processing & Petrochemical Technology, 2023, 25(03): 136-152.

[32] Yang K-R, Dai J-Y, Wang S-P, et al. Bio-based epoxy composites demonstrating high temperature breakdown strength and thermal conductivity for high voltage insulation[J]. Chinese Journal of Polymer Science, 2025, 43(1): 40-52.